Absolute and convective instabilities of natural convection flow in boundary-layer regime

J. Tao*
BP Institute, Bullard Laboratories, University of Cambridge, Cambridge, CB3 0EZ, United Kingdom

P. Le Quéré and S. Xin
L.I.M.S.I.-C.N.R.S., Boîte Postale 133, 91403 Orsay Cedex, France

(Received 16 March 2004; revised manuscript received 13 September 2004; published 28 December 2004)

The spatiotemporal instability of the buoyancy-driven flow adjacent to a vertically heated wall, which is immersed in thermally stratified medium, is studied theoretically and numerically. The temperature gradients ratio between the wall and the ambient fluid is shown to lead to rich scenario of absolute-convective instability transitions. The direct numerical simulations consistent with the theoretical prediction are presented. The supercritical steady state, found in previous simulations of the natural convection in vertically heated square cavity, is explained in terms of the convective instability, and the nonlinear effect on the convectively unstable waves is discussed as well.

DOI: 10.1103/PhysRevE.70.066311 PACS number(s): 47.20.Bp, 47.55.Hd

I. INTRODUCTION

The buoyancy-induced natural convection flow contiguous to a heated vertical wall is a fascinating problem in fluid mechanics and thermal physics literature. Mostly, temperature defect and flow reversal are formed in such boundary layer when the ambient fluid is thermally stratified. In past theoretical studies, only two kinds of boundary conditions were considered: isothermal plate and plate dissipating uniform heat flux. The similarity solution for uniform heat flux case was studied first, because its steady state is a simple parallel flow [1–6]. A good example for such boundary layer is the sidewall layer in a square cavity with vertical walls transfering uniform heat flux. While the similarity solution [7] and the corresponding instability properties [8] for isothermally heated plate were obtained much later, because the convection is spatially developing flow, where the downstream variation of the flow field must be considered. Kimura and Bejan [6] studied the natural convection in rectangular cavity with uniform heat flux boundary condition, and concluded that the core fluid must be motionless and linearly stratified. Afterwards, numerical simulations confirmed their conclusions, and linear instability analyses were also carried out [9]. However, a strange phenomenon was found in numerical simulations: the flow field tends to converge to a steady state, the supercritical steady state, though the Grashof number is much larger than the linear critical value [10]. It was presumed that this tendency may be caused by the convectively unstable properties of the flow, and the flow may transfer to be absolutely unstable at higher Grashof number. However, serious efforts have not yet been made.

The convective and absolute instabilities in shear flows have attracted increasing attention not only because of their crucial importance for flow control but also for the fundamental interest to understand the various processes leading from laminar flow to turbulence [11–14]. In convectively unstable flow, the amplified disturbances move away from the source (e.g., forced flat boundary-layer flow); while in absolutely unstable flow, the growing wave packet expands around the source and its frequency is insensitive to low noise levels (e.g., the Kármán vortex street). The distinction requires a fully spatiotemporal analysis, which was first used in plasma instability [15], and more recently applied to natural convection flows [8,16]. Forced laminar flat-plate boundary layer was investigated and found the transient response to correspond to convective instability [17]. While for natural convection boundary layer near an isothermal wall, Krizhevsky *et al.* [8] found that the flow turned from convective unstable into absolute unstable at a critical Grashof number, which increased with the Prandtl number. However, whether there is absolute instability for uniform heat-flux boundary layer, which is a more appropriate model than the isothermal one for solar applications, is unclear at present, and this fact is the principal motivation behind the present study.

The outline for the remainder of this paper is as follows. First, we present a similarity solution for the boundary-layer flow, including previous steady state solutions as its special cases. Second, it is discussed how the fluid property and the background thermal stratification affect the convective-absolute instability transition. Third, a quantitative comparison between the direct numerical simulation and the theoretical analysis is made by the examination of frequency and wave number of the fluctuating waves. A concluding discussion is given in the final section.

II. GOVERNING EQUATIONS

The boundary layer to be considered here differs from previous ones in that the temperature of the vertical heated plate $T^*_w(x)$ and the ambient fluid $T^*_\infty(x)$ have *independent* vertical temperature gradients N_w and N_∞, say, $T^*_w(x^*) = T^*_w(0) + N_w x^*$, $T^*_\infty(x^*) = T^*_\infty(0) + N_\infty x^*$, $T^*_w(0) - T^*_\infty(0) = \Delta T(0) > 0$ (see Fig. 1). The coordinate x^* is measured ver-

*Author to whom correspondence should be addressed. Email address: tao@bpi.cam.ac.uk

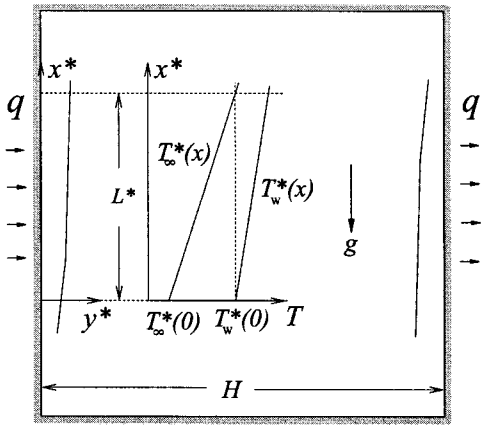

FIG. 1. Sketch of the setup. Note that the boundary layers are not drawn in real scale, because they are very thin in reality. q is heat flux. For details see text.

tically and opposite to the direction of gravity acceleration g, and y^* is the coordinate normal to the surface (stars indicate dimensional quantities). The subscript "∞" denotes the ambient condition, and $\Delta T(0)$ is the temperature difference between the plate and the background fluid at $x^*=0$. After introducing a parameter a, which is the ratio between the temperature gradients N_w and N_∞, we can obtain a similarity solution, and by which a variety of cases from the isothermal to the uniform-heat-flux boundary conditions can be analyzed within a single framework.

In order to get a stable thermally stratified medium, we assume $N_\infty > 0$ and $N_w \geqslant 0$. In addition, the plate is assumed to be of finite extent, and its temperature is above the surrounding fluid at any elevation. L^* is a long length scale where $T^*_\infty(L^*) = T^*_w(0)$. The Grashof number Gr and the Prandtl number Pr are defined as $[g\beta\Delta T(0)L^{*3}/\nu^2]^{1/4}$ and ν/κ, and the temperature ϕ, coordinates (X,Y), time τ, and pressure P are dimensionalized as $[T^*(x^*) - T^*_\infty(x^*)]/[T^*_w(x^*) - T^*_\infty(x^*)]$, $(x^*, y^*)\mathrm{Gr}/L^*$, $\tau^* \nu \mathrm{Gr}^3/L^{*2}$, and $[P^* - P_\infty(x^*)]L^{*2}/(\rho\nu^2\mathrm{Gr}^4)$, where ρ, ν, κ, and β are the fluid density, the kinematic viscosity, the thermal diffusivity and the coefficient of thermal expansion. By applying the Boussinesq assumption, we obtain the governing dimensionless continuity, momentum and energy equations

$$\begin{cases} \dfrac{\partial U}{\partial X} + \dfrac{\partial V}{\partial Y} = 0 \\ \dfrac{\partial U}{\partial \tau} + U\dfrac{\partial U}{\partial X} + V\dfrac{\partial U}{\partial Y} = -\dfrac{\partial P}{\partial X} + \dfrac{1}{\mathrm{Gr}}\nabla^2 U + \dfrac{1}{\mathrm{Gr}}\phi[1 + (a-1)\varepsilon X] \\ \dfrac{\partial V}{\partial \tau} + U\dfrac{\partial V}{\partial X} + V\dfrac{\partial V}{\partial Y} = -\dfrac{\partial P}{\partial Y} + \dfrac{1}{\mathrm{Gr}}\nabla^2 V \\ \dfrac{\partial \phi}{\partial \tau} + U\dfrac{\partial \phi}{\partial X} + V\dfrac{\partial \phi}{\partial Y} = \dfrac{1}{\mathrm{PrGr}}\nabla^2\phi - \dfrac{U[1 + (a-1)\phi]}{\mathrm{Gr}[1 + (a-1)\varepsilon X]} + \dfrac{2(a-1)}{\mathrm{PrGr}^2}\dfrac{\partial \phi}{\partial X} \end{cases} \tag{1}$$

with boundary conditions:

$$U(\tau,X,0) = V(\tau,X,0) = 1 - \phi(\tau,X,0) = \phi(\tau,X,\infty) = U(\tau,X,\infty) = P(\tau,X,\infty) = 0, \tag{2}$$

where the operator $\nabla^2 = \partial^2/\partial X^2 + \partial^2/\partial Y^2$, and $\varepsilon = 1/\mathrm{Gr}$, characterizes the degree of spatial inhomogeneity of the basic flow. As shown in Eq. (2), no-slip boundary condition for velocity is used on the wall, while in the far field the vertical velocity is diminished.

The following forms of stream function φ_0, horizontal length scale η, and temperature H_0 are proposed (subscript "0" refers to the basic flow) in order to get a similarity solution

$$\varphi_0(X,Y) = 2\sqrt{2}[1 + (a-1)\varepsilon X]F_0(\eta), \quad \eta = Y/\sqrt{2},$$

$$\phi_0(X,Y) = H_0(\eta), \tag{3}$$

then the velocities in the boundary layer are given by

$$U_0 = \frac{\partial \varphi_0}{\partial Y} = 2[1 + (a-1)\varepsilon X]F_0{}',$$

$$V_0 = -\frac{\partial \varphi_0}{\partial X} = -2\sqrt{2}(a-1)\varepsilon F_0. \tag{4}$$

Since the velocity component includes the coordinate X, the boundary-layer flow is slowly spatially developing flow except for a special case $(a=1)$.

Employing the boundary-layer approximation and the earlier transformations to Eqs. (1) and (2), the steady basic flow can be described by the following ordinary differential equations:

$$\begin{cases} F_0{}''' + 4(a-1)F_0F_0'' - 4(a-1)(F_0{}')^2 + H_0 = 0 \\ \dfrac{1}{\mathrm{Pr}}H_0'' + 4(a-1)F_0H_0{}' - 4F_0{}'[1 + (a-1)H_0] = 0 \end{cases} \tag{5}$$

with boundary conditions

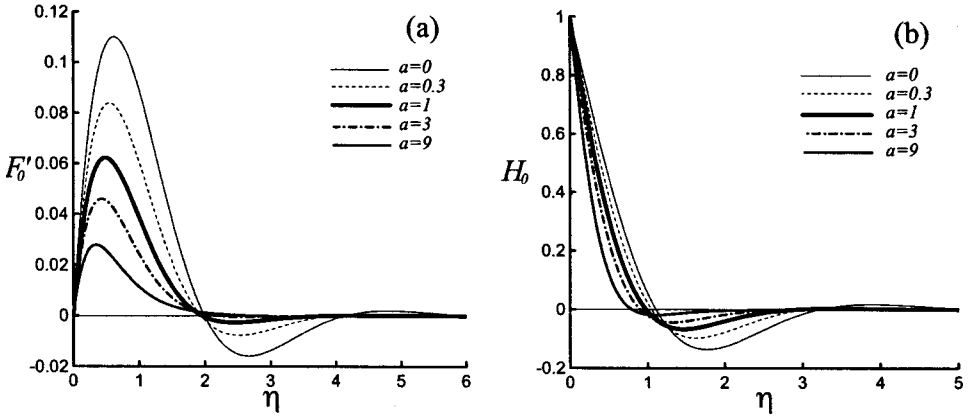

FIG. 2. The cross-stream profiles of dimensionless vertical velocity (a) and temperature (b) as functions of the temperature gradient ratio a for Pr=6.7.

$$F_0(0) = F_0'(0) = 1 - H_0(0) = F_0'(\infty) = H_0(\infty) = 0. \quad (6)$$

The interesting point of the similarity solution supported by the earlier equations is: when $a=0$ or $N=0$, we get $T^*_w(x)=T^*_w(0)$, hence, the wall is isothermally heated, and the equations reduce to the ones used by Krizhevsky *et al.* [8]; while $a=1$, the wall and the ambient fluid have the same vertical temperature gradient. Consequently the local heat flux dissipated from the plate is

$$q(x^*) = -\lambda \left.\frac{\partial T^*}{\partial y^*}\right|_{y^*=0} = -\frac{\lambda}{\sqrt{2}L^*}\left.\frac{\partial H_0}{\partial \eta}\right|_{\eta=0} [T^*_w(0) - T^*_\infty(0)][\mathrm{Gr} + (a-1)X], \quad (7)$$

which represents a uniform-heat-flux boundary condition as a is unit. Here λ is the conductivity of the fluid. By simple transformation, the ordinary differential equations for $a=1$ can be reduced easily to the same form as discussed previously [4,6]. Therefore, present similarity solution makes it possible to study the flow fields continuously from the uniform-heat-flux wall to the isothermal wall just by varying the temperature gradient ratio a. Equations (5) and (6) are resolved by forth-order Runge-Kutta procedure and shooting method.

It is shown in Fig. 2 that the steady basic flow has reversals and temperature defects for both the isothermal $(a=0)$ and the uniform-heat-flux $(a=1)$ boundary conditions. Larger a means less influence of the stratified background on the flow field. When $a=9$ no flow reversal can be found in the velocity profile, though the temperature defect still exists. In fact the flow reversal is difficult to find after $a>5$ for Pr=6.7.

The instability analysis is focused on the transition between the two typical boundary conditions $(0\leqslant a\leqslant 1)$ and in the range $0\leqslant \varepsilon X<1$ $(0\leqslant x^*<L^*)$. The following forms of disturbance stream function and temperature are employed (subscript "1" refers to the disturbance field):

$$\varphi_1 = 2\sqrt{2}[1 + (a-1)\varepsilon X]\Psi_1(\eta)\exp[i(k_1 X - \omega_1 \tau)],$$
$$\phi_1 = \Phi_1(\eta)\exp[i(k_1 X - \omega_1 \tau)], \quad (8)$$

and the Orr-Sommerfeld equation coupled with energy equation can be obtained according to stability theory

$$\begin{cases} (\Psi_1'' - k^2\Psi_1)\left(F_0' - \dfrac{\omega}{k}\right) - F_0'''\Psi_1 = \dfrac{1}{ikG}\{\Psi_1'''' - 2k^2\Psi_1'' + k^4\Psi_1 + \Phi_1'\} \\ \left(F_0' - \dfrac{\omega}{k}\right)\Phi_1 - H_0'\Psi_1 = \dfrac{1}{ikG\mathrm{Pr}}(\Phi_1'' - k^2\Phi_1) \end{cases} \quad (9)$$

with the boundary conditions

$$\Psi_1(0) = \Psi_1'(0) = \Phi_1(0) = \Psi_1(\infty) = \Psi_1'(\infty) = \Phi_1(\infty) = 0, \quad (10)$$

where

$$G = 2\sqrt{2}\mathrm{Gr}[1 + (a-1)\varepsilon X], \quad k = \sqrt{2}k_1,$$

$$\omega = \frac{\omega_1}{\sqrt{2}[1 + (a-1)\varepsilon X]}.$$

The modified Grashof number, wave number and frequency G, k, and ω are introduced only to simplify the equations. It is noted that in order to deduce the earlier equations some additional terms are ignored as $G^{-1}\gg 1$, and this condition is satisfied well in all instability problems discussed later.

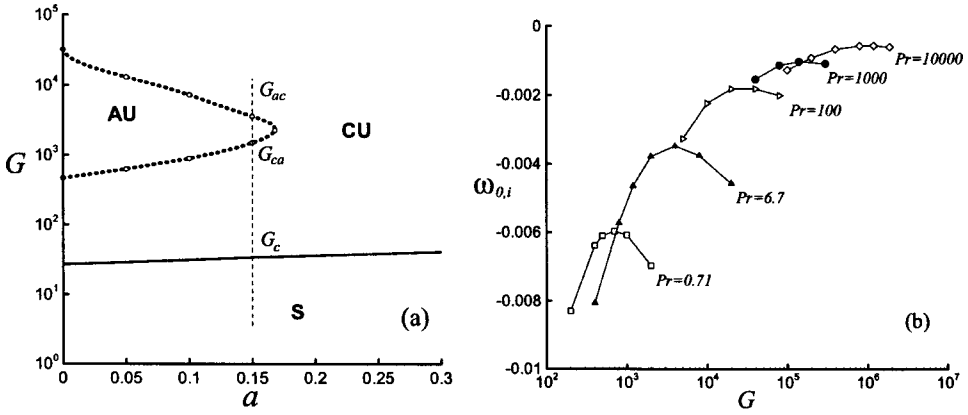

FIG. 3. (a) The convective/absolute instability boundary for Pr=6.7. AU, absolutely unstable; **CU**: convectively unstable and **S**: stable. (b) The modified absolute growth rate $\omega_{o,i}$ as a function of G for different Prandtl numbers with uniform-heat-flux boundary condition $a=1$.

In Sec. III we carry out a fully spatiotemporal stability analysis. Consequently both the modified wave number k and frequency ω of the disturbances are taken as complex numbers. The boundary conditions at infinity are replaced by Nachtsheim's asymptotic forms [18] at a finite cross-stream distance η_{max} for numerical reasons. The coupled disturbance Eqs. (9) and (10) are discretized with fourth-order finite difference scheme at n uniformly distributed points in the η interval [0, η_{max}]. The resulting amplitude equations define an algebraic system $\mathbf{A}(\Psi_1,\Phi_1)=0$ with sparse $2n\times 2n$ complex matrix A. The homogeneous equation admits nonzero solutions for Ψ_1 and Φ_1 if and only if the determinant of **A**:

$$|\mathbf{A}(k,\omega,G)| = |\mathbf{A}(k,\omega,\mathrm{Gr},X_g)| = 0. \tag{11}$$

Based on the earlier relation a variable (e.g., the complex k) can be resolved by the predictor-corrector method after all the remaining variables are specified. In order to achieve numerical accuracy of the results, a high enough number of points n and a large enough η_{max} must be chosen. In this paper, the result is required to vary by no more than 0.1% when increasing η_{max} to $1.5\eta_{max}$. As a consequence, $\eta_{max}<7\eta(F_0{}'_{max})$ is used for all subsequent calculations. The grid point number is determined when the absolute value of the result varies by less than 10^{-8} on doubling the grid points. The numerical methods described here have been used to study the absolute instability in vertical heated slot [16], and tested successfully against the results of previous researches [8,19].

III. SPATIOTEMPORAL INSTABILITY

The wave number observed along the ray $X/\tau=0$ at a fixed spatial location in a laboratory frame is defined by the zero-group-velocity

$$\frac{\partial\omega}{\partial k}(k_0) = 0, \tag{12}$$

and $\omega_o=\omega(k_0)$. The real part $\omega_{o,r}$ is referred as the absolute frequency and the imaginary part $\omega_{o,i}$ is denoted the absolute growth rate. The Briggs-Bers criterion is used to distinguish absolute and convective instabilities: the flow is convectively unstable (CU) if $\omega_{o,i}<0$ and absolutely unstable (AU) if $\omega_{o,i}>0$. Moreover, the saddle point described by Eq. (12) must be a pinching point between two distinct spatial branches $k+$ and $k-$ (k complex and ω_i constant) originating from distinct halves of the k plane when ω_i is decreased. This condition is systematically checked in present work.

It is shown in Fig. 3(a) that when the modified Grashof number G is less than the critical value G_c, the flow is stable. At higher G ($G_c>G>G_{ca}$), the flow becomes convectively unstable. For small a (e.g., $a=0.15$), it is illustrated intriguingly that the flow turns to be absolutely unstable when $G_{ca}<G<G_{ac}$. The G_{ca} and G_{ac} are the critical Grashof numbers defining the convective-absolute and the absolute-convective instability transitions. The existence of G_{ca} for isothermal wall ($a=0$) was reported before [8], but the researchers did not explore higher Grashof number to find the G_{ac}. Figure 3(a) also shows that the absolutely unstable region becomes smaller at larger a, and after a is larger than 0.17 the flow system does not support the absolutely unstable modes for Pr=6.7 (water). Since it is well known that the absolute unstable mode can be self-excited and behaves as an oscillation source, the laminar-turbulence transition is much easier for absolutely unstable flow than for convectively unstable one. Therefore, the importance of the present result [Fig. 3(a)] is that it provides a new mechanism for us to control the flow state and heat transfer: increasing a when we want to keep the flow laminar and decrease heat dissipation, or decreasing a if we hope it to be turbulent.

When $a=1$, it is shown in Fig. 3(b) that enlarging Prandtl number increases $(\omega_{o,i})_{max}$. However, the flow remains convectively unstable even Pr reaches as high as 10 000, where the solutions should be very close to their asymptotic limits. This result confirms the first part of past conjecture: the flow with uniform heat flux boundary is convectively unstable, but denies the second part at least in the view of linear theory: the existence of absolute instability.

In order to analyze an isothermal boundary layer, Krizhevsky *et al.* [8] defined a velocity ratio R, the ratio between the absolute values of the minimum and the maximum in the vertical velocity profile, and concluded that as R increased the flow was more susceptible to be absolutely unstable. In present case, our interest mostly lies in $a\in[0,1]$, and smaller a means larger downstream variation of the temperature difference between the wall and the ambient

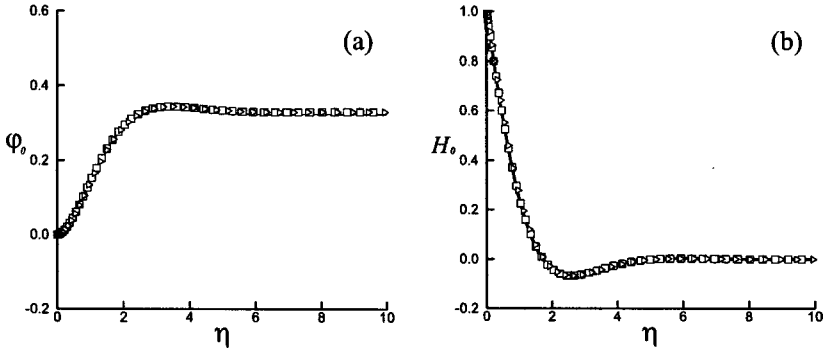

FIG. 4. Comparison of (a) stream function and (b) temperature between the similarity solutions for $a=1$ (solid line) and the numerical results obtained for Gr $=23.2$ (□) and Gr$=27.8$ (▷). The simulation data are calculated at the centerline ($x^*=0$) when the flow reaches its steady state.

fluid at the same elevation, which leads to stronger reverse flow. As a result, larger R corresponds to smaller a [see Fig. 2(a)], and according to the earlier analysis the flow is more yielding to the absolute instability. Therefore, our results are in consistent with the conclusion of Krizhevsky *et al.*

IV. DIRECT NUMERICAL SIMULATION

In this section we compare our theoretical results with direct numerical simulations of the natural convection flow in a square cavity filled with air, whose vertical sidewalls dissipate uniform heat flux while the top and bottom ends are adiabatic (see Fig. 1). When the heat flux is large, two boundary-layer regimes will form near the vertical walls, while the core fluid is motionless and the core temperature varies linearly in vertical direction. Gill [4] studied such buoyancy layer and found an asymptotic solution, which is just a special case ($a=1$) of the present similarity solution.

Based on the Boussinesq assumption, the complete Navier-Stokes equation coupled with energy equation is integrated by a pseudospectral algorithm, and no-slip boundary condition is used for velocity on all walls. A spatial expansion in series of Chebyshev polynomials and a semi-implicit second-order finite-difference time-marching scheme are used. The Helmholtz equations arising from time discretization are solved with the tau method and the partial diagonalization algorithm [20]. The incompressibility condition is treated by the use of an influence matrix technique [21,22]. Spatial resolution 257×385 is used in order to obtain high accuracy. For the sake of brevity, the details of the algorithm are not reproduced here.

Conveniently, the origin of the coordinates is chosen at the center of the left vertical wall. The asymptotic relation for $\mathrm{Pr}\ll1$ between the length scale L^* and the width of the square cavity H can be obtained according to Kimura and Bejan's analysis [6]:

$$\frac{H}{L^*}=\frac{1}{2\sqrt{2}}\mathrm{GrPr}^{1/4}. \tag{13}$$

Although the earlier relation was obtained for large Prandtl number, it was concluded that the Prandtl number does not have a significant influence on solution as long as Pr is $0(1)$ or greater [7]. In our numerical simulation Pr$=0.71$, and it is shown in Fig. 4 that when the flow reaches a steady state, the numerical data for temperature and stream function agree very well with the similarity solutions. Since the unstable modes will grow up from small disturbances to saturated states, a natural question that needs to be answered is how the nonlinear process affects their spatiotemporal properties.

In order to study the nonlinear effect, we choose Gr$=45$, which is nearly two times larger than the critical value ($\mathrm{Gr}_{crit}=24$ for Pr$=0.71$). The initial disturbance is introduced by using a solution obtained for a different Grashof number as the initial field. Since the flow in the boundary-layer regime is almost parallel in vertical direction, the nonuniform disturbances arise near the cavity corners. The temporal evolutions of the horizontal velocity V at fixed points are shown in Fig. 5. It is illustrated that the initial disturbances trigger regular fluctuating waves that drift downstream. The oscillating frequency and the maximum amplitude of these waves increase in the downstream direction, and reach some finite values at last.

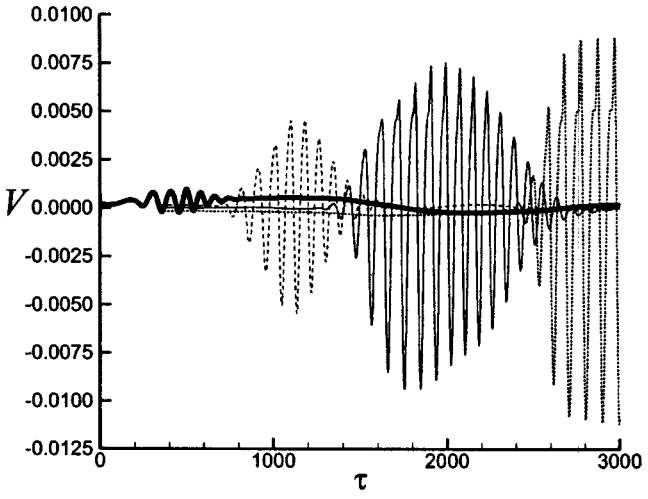

FIG. 5. Time traces of horizontal velocity for Gr$=45$ at several locations in the boundary-layer regime. The thick solid line, dashed line, solid line, and dotted line indicate data at points $(x^*/H, y^*/H)=(-0.3649, 0.0014)$, $(-0.1989, 0.0014)$, (0, 0.0014), and (0.3649, 0.0014).

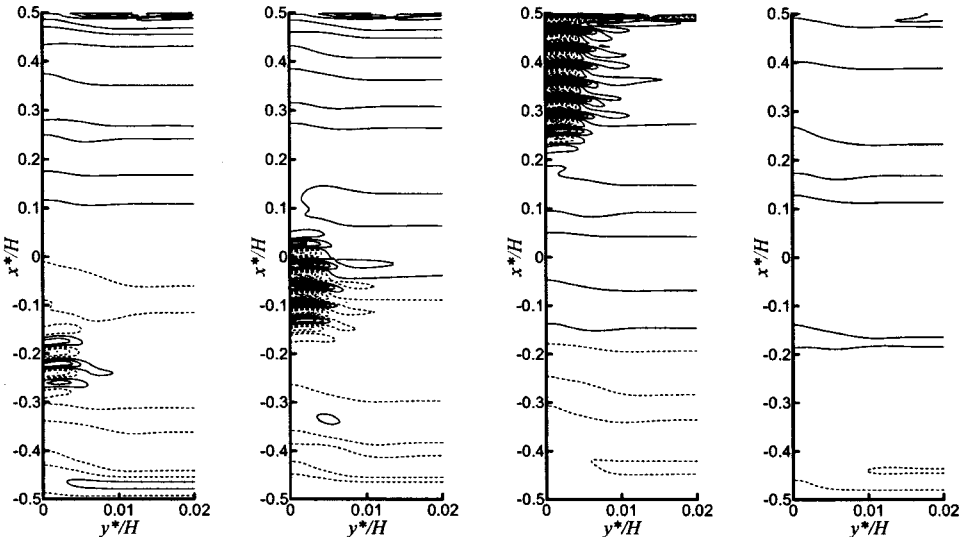

FIG. 6. Isocontours of the disturbing temperature field $\phi(\tau) - \phi_{ref}$ near the left wall for Gr $=45$ at $\tau=1050$, 1650, 3850, and 9700 (from left to right). ϕ_{ref} is the temperature field of supercritical steady state obtained at $\tau = 24\,000$. Solid (dashed) lines indicate positive (negative) values except for the solid line adjacent to the dashed lines that indicates zero.

The spatial structure of the disturbing temperature field is shown in Fig. 6. Arising near the left-bottom corner, the spatially amplified wave packet is swept downstream and develops to a saturated state. This is a typical feature of convective instability. A close examination can find that the wavelength becomes short during the nonlinear evolution. After blocked by the top boundary at the left-top corner, the saturated waves are damped. Since there is no mechanism in a closed cavity to feed perturbations at the upstream part of the boundary-layer regime, as shown in Fig. 6 for $\tau=9700$, the disturbing field tends to vanish after long time iteration. The flow near the right vertical wall shows similar phenomena as revealed in Fig. 6 except the orientation: the wave packet drifts from top to bottom and is damped at the right-bottom corner.

Since the fluctuating waves present convectively unstable properties obviously, we compare them with analytical solutions obtained by using spatial mode, where the frequency ω is looked as real and k is taken as complex. It is shown clearly in Fig. 7 that at the first stage of instability, the frequency and wave number of the fluctuating wave coincide well with the values of the convectively unstable mode with the largest spatial growth rate. According to present numerical simulations, we can also conclude that, although the nonlinear effect leads to the increase of the wave number and the frequency, the flow in the boundary-layer regime still remains convectively unstable.

V. CONCLUSIONS

The instability properties of natural convection in the boundary-layer regime with thermal stratification background have been investigated theoretically and numerically.

By introducing a parameter a, the temperature gradient ratio between the wall and the ambient fluid, we obtain a similarity solution, which includes previous solutions as its special cases. Based on an instability analysis with the coupled Orr-Sommerfeld equation and the energy equation, it is shown that the temperature gradient ratio has dramatic influence on the spatiotemporal properties of the flow. For small a, the flow may change from convectively unstable to absolutely unstable as $G_{ca} > G > G_{ac}$, and will turn to be convectively unstable again when $G > G_{ac}$. These instability transitions not only reveal a mechanism to control the flow state, but also provide an ideal model for further study of the global instability [14], which exists wherever local absolute instability occurs for spatially developing flows.

According to the instability theory, only convectively unstable mode exists when a is large (e.g., $a=1$). This prediction is consistent with our numerical result about the boundary-layer regime in a square cavity. When the flow is steady, the numerical data for velocity and temperature agree well with the similarity solutions. When disturbances are introduced, the convectively unstable mode with the largest growth rate will develop first and dominate the flow pattern.

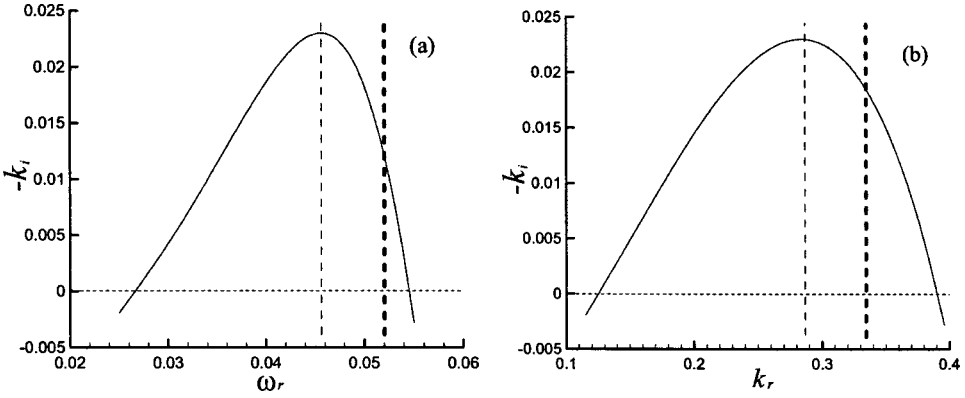

FIG. 7. The theoretical growth rate of convectively unstable mode as a function of (a) frequency ω_r and (b) wave number k_r for Gr$=45$. The thin vertical dashed lines indicate the initial state of the fluctuating wave found in numerical simulation, and the thick dashed lines indicate its finite-amplitude state near the left-top corner.

The spatially amplified wave packet drifts downstream, and its frequency and wave number increase due to nonlinear effect. Since the convectively unstable waves are damped at the corner and no other disturbing sources exist in the closed cavity, the whole flow field will converge finally to the supercritical steady state.

ACKNOWLEDGMENTS

The computations were performed on the NEC-SX5 at IDRIS, and this work was supported by French Ministry of Research and New Technologies. The authors are grateful for Dr. I. Delbende's fruitful discussions.

[1] L. Prandtl, *Essentials of Fluid Dynamics* (Blackie, London, 1952), p. 422.
[2] P. A. Iyer, Boundary-Layer Meteorol. **5**, 53 (1973).
[3] P. A. Iyer and R. E. Kelly, J. Heat Transfer **100**, 648 (1978).
[4] A. E. Gill, J. Fluid Mech. **26**, 515 (1966).
[5] A. E. Gill and A. Davey, J. Fluid Mech. **35**, 775 (1969).
[6] S. Kimura and A. Bejan, J. Heat Transfer **106**, 98 (1984).
[7] K. Kulkarni, H. R. Jacobs, and J. J. Hwang, Int. J. Heat Mass Transfer **30**, 691 (1987).
[8] L. Krizhevsky, J. Cohen, and J. Tanny, Phys. Fluids **8**, 971 (1996).
[9] G. Desrayaud, Rep. CNAM 1990/LT/01, 1990.
[10] P. Le Quéré, in *Proceedings of the 10th International Heat Transfer Conference*, Brighton, (IChemE, Rugby, England, 1994), pp. 281–296.
[11] P. A. Monkewitz, P. Huerre, and J.-M. Chomaz, J. Fluid Mech. **251**, 1 (1993).
[12] I. Delbende and J. Chomaz, Phys. Fluids **10**, 2724 (1998).
[13] B. Pier and P. Huerre, J. Fluid Mech. **435**, 145 (2001).
[14] P. Huerre, *Perspectives in Fluid Dynamics, A Collective Introduction to Current Research* (Cambridge University Press, 2000), Chap. 4.
[15] R. J. Briggs, *Electron-Stream Interaction with Plasmas* (MIT Press, Cambridge, MA, 1964).
[16] J. Tao and F. Zhuang, Phys. Rev. E **62**, 7957 (2000).
[17] M. Gaster, Phys. Fluids **11**, 723 (1968).
[18] P. R. Nachtsheim, NACA, TN D-2098, 1963.
[19] B. A. Brewster, J. Fluid Mech. **229**, 115 (1991).
[20] D. Haidvogel and T. Zang, J. Comput. Phys. **30**, 167 (1979).
[21] P. Le Quéré, Comput. Fluids **20**, 29 (1991).
[22] P. Le Quéré and M. Behnia, J. Fluid Mech. **359**, 81 (1998).